

## Chapter 4

### Theory of Digital holography

#### 4.1 Recording of Holograms

The first step in holography is recording of the hologram or the interference patterns which arises due to the overlapping of the reference and object wavefronts (Fig 4.1), on a digital array [66–68,174,182,261–263]. The amplitude and phase information of the object under investigation are both present in this interference pattern. [67,194]. Common-path self-referencing off axis digital holographic geometries are used in all the developed techniques and applications in this thesis. The region of the hologram where the object information is missing acts as a reference wave in self-referencing geometry [52,54,58,64,80,84,264]. Use of common path self-referencing geometries enables one to achieve a compact setup using minimal optical components and higher temporal stabilities and also allows the use of LED (a low coherent source) as the illumination source. In Self-referencing off-axis geometries, the object beam is split into two and pass through the same components and travel the same path giving rise to interference fringes which are recorded using a digital sensor [52,64,65,80] as shown in Fig 4.1

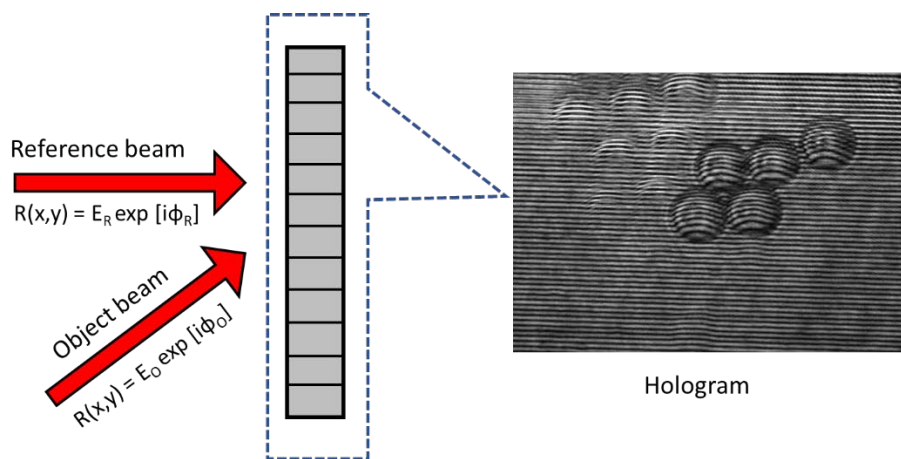


Fig 4.1 Formation of hologram due to superposition of the object and the reference wavefronts at the detector plane. Carrier fringes are modulated in the region where the object exists.

Photodetectors are quadratic in nature, and they only respond to intensity distributions. As a result, the interference pattern is recorded as a spatially varying intensity distribution on the recording medium [54,63,67,174,182,206,265–268]. The complex amplitude distributions of the object and reference wavefronts at the recording plane (hologram plane) are  $O(x, y) = E_o(x, y) \exp[i\phi_o(x, y)]$  and  $R(x, y) = E_r(x, y) \exp[i\phi_r(x, y)]$  respectively (where  $E_o$

and  $E_R$  are their respective scalar amplitude distributions and  $\phi_o$  and  $\phi_R$  are their respective phase distributions), then the resulting intensity profile (hologram) imaged by the digital sensor can be denoted by the following equation[206]

$$I_H(x, y) = |O + R|^2 = (O + R)(O + R)^* \\ = (E_o \exp[i\phi_o] + E_R \exp[i\phi_R])(E_o^* \exp[-i\phi_o] + E_R^* \exp[-i\phi_R]) \quad (4.1)$$

where \* denotes the complex conjugation.

Eq. (4.1) can be simplified in terms of the intensities of the object and reference wavefronts

$$I_H(x, y) = E_o E_o^* + E_R E_R^* + E_o E_R^* \exp[i(\phi_o - \phi_R)] + E_R E_o^* \exp[-i(\phi_o - \phi_R)] \\ = I_o + I_R + E_o E_R^* \exp[i(\phi_o - \phi_R)] + E_R E_o^* \exp[-i(\phi_o - \phi_R)] \quad (4.2)$$

$I_o$  and  $I_R$  represent the intensity of the object and reference beam respectively. Collectively ( $I_o + I_R$ ) may be regarded as the background terms [206].

## 4.2 Reconstruction of Holograms

The reconstruction of the recorded hologram is the second step in holography. Holograms are reconstructed in traditional holography by illuminating them with the actual reference beam, whereas they are reconstructed in digital holography by illuminating them with an exact digital replica of the reference wave. This is numerically equivalent to multiplying Eq (4.2) by the reference wave [67,269].

$$I_H(x, y) E_R \exp[i\phi_R(x, y)] = (I_o + I_R) E_R \exp[i\phi_R] \\ + I_R E_o \exp[i\phi_o] + E_R E_R \exp[2i\phi_R] E_o^* \exp[-i\phi_o] \quad (4.3)$$

In Eq. (4.3) the undiffracted term advances through the hologram (zero order) is represented by the first term [66] which does not contain any information about the object. The second term represents the object wave's complex amplitude information (at the hologram plane), which can be propagated to the image plane to obtain object information. This is also called the virtual image (since it is formed exactly at the position where the object existed and is an exact replica of the object). The distorted real image of the object is represented by the last term on the RHS. In off-axis digital holography, the three terms in Eq. (4.3) are separated at the hologram plane as well as at the image plane (Fig. 4.2). From Eq. (4.3) it can be seen that by illuminating the digital hologram with a numerical reference wave and propagating it to the image plane, the complex amplitude (which includes both scalar amplitude and phase information of the object) can be obtained.

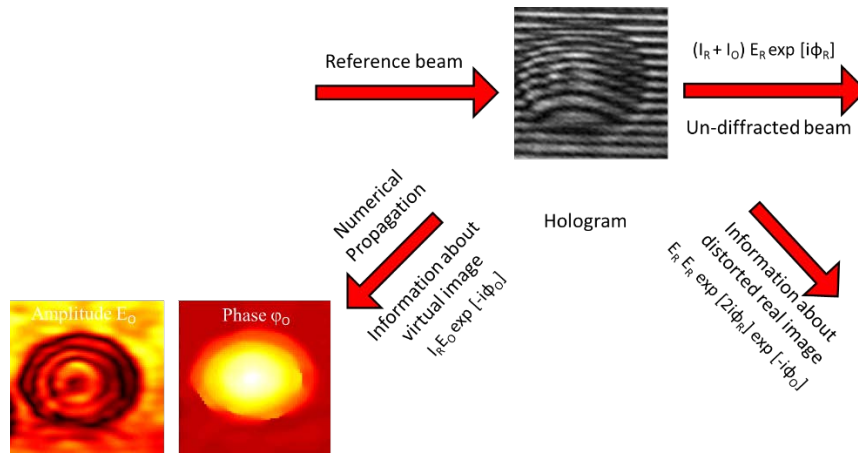


Fig 4.2 Digital hologram reconstruction. Reference wave gets scattered from the structures of the hologram. It is numerically propagated to the position where the object existed (virtual image)

The object wave field is computed using scalar diffraction theory to simulate the diffraction of the reference wavefront from the interference fringes of digitally recorded holograms [67,182]. The Fresnel–Kirchhoff diffraction integral with Fresnel transform after Fresnel approximation can be used in this process [270–272]. The angular spectrum propagation (ASP) approach to scalar diffraction theory can also be used to perform reconstruction [273–276]. Each of these methods describes how the reconstructing wave scatters (diffraction) from the hologram's structures (interference fringes) and how the scattered wavefront propagates to the image plane. The complex amplitude distribution of the sample under examination is obtained through the numerical reconstruction process. The intensity distribution and phase (thickness) of the object are both represented by complex amplitude. The best approach to retrieve the object complex amplitude distribution is to use the Fresnel-Kirchoff integral with Fresnel approximation (where the distance of propagation is very large compared to the size of the hologram and we assume paraxial approximation) [270,271].

The image of the magnified object in digital holographic microscopy (DHM) is either at the detector plane or very close to the detector plane (Fig. 4.3). The propagation step can also be bypassed if the hologram plane (detector) is kept in the magnifying lens' image plane [78–80,260,277]. ASP approach represents the wavefront propagation over small distances with respect to the size of the array (hologram). The Fresnel-Kirchoff integral, on the other hand, assumes that the propagation distance is very large compared to the hologram dimensions. As a result, the ASP approach is appropriate for image reconstruction in the case of DHM. It also helps to keep the system compact. One of the features of this technique is that it can differentiate the various diffracted components (un-diffracted reference, virtual, and real) in

the frequency domain, ensuring that none of these components in the reconstruction plane overlap (image plane) [273].

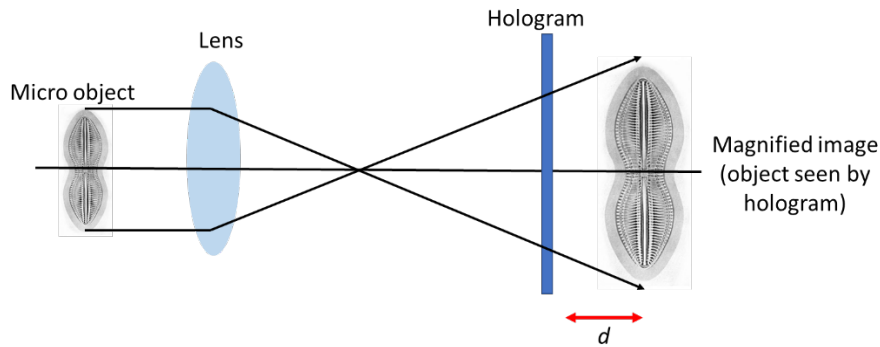


Fig 4.3 Position of the object (magnified image) and the hologram (detector) plane in DHIM. The object plane (magnified image plane) is situated either at the detector or very near to it.

### 4.3 Numerical propagation using Angular Spectrum approach

As shown in Fig. 4.4, waves scattering from an object under investigation can be thought of as plane wave components propagating in different directions (angles). The scattering angle of the object wavefront depends upon the object spatial frequency distribution. By summing (integrating) the contributions due to these plane wave components, the complex amplitude of the wavefront in another parallel plane can be computed [182].

For retrieving complex amplitude distribution of the object using ASP approach (Fig. 4.5), digital holograms as the reference wave illuminates it, giving rise to the complex amplitude at the hologram plane, which is can be written as follows [63]

$$U(x, y, z=0) = I_H(x, y) E_R \exp[i\phi_R(x, y)] \quad (4.4)$$

In Eq. (4.4),  $z=0$  is the hologram plane and  $U(x, y, z=0)$  is the complex amplitude at the hologram plane due to illumination of the hologram by the reference wavefront. The aim of the numerical processing is to propagate this complex amplitude distribution to the plane, where the object (magnified image) existed.

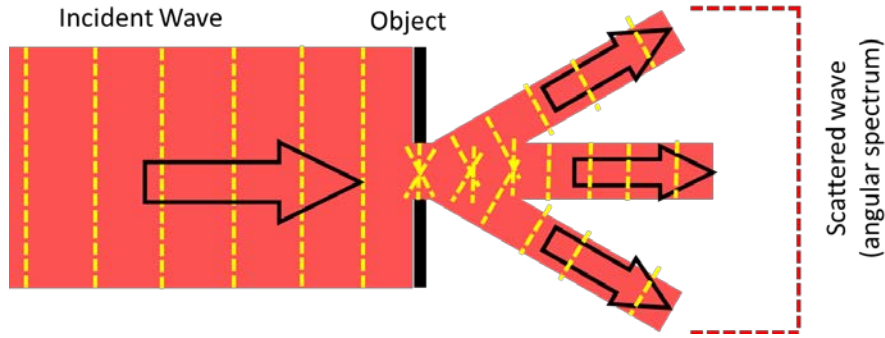


Fig 4.4 Scattered wavefront as a collection of plane waves travelling in different directions (angle). The scattering angle is decided by the spatial frequency of the object (smaller objects, higher spatial frequencies) scatter at higher angles. An object with sinusoidal intensity variation (like a hologram), will give rise to only three scattered components (only one frequency component)

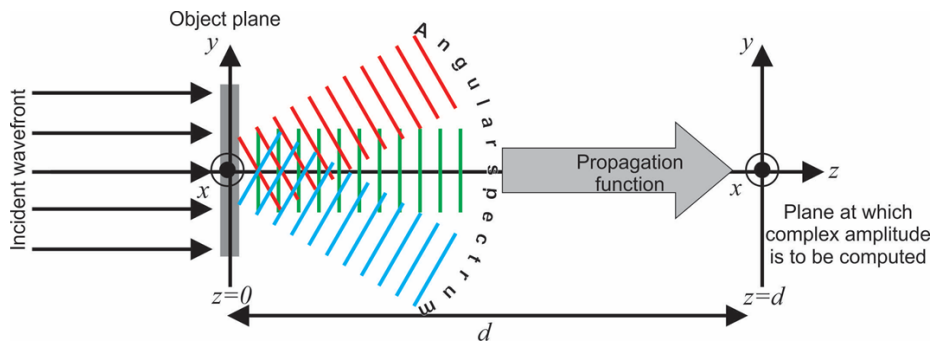


Fig 4.5 Numerical reconstruction of digital holograms using ASP approach. Reference wave illuminating the hologram generates the angular spectrum at the hologram plane ( $z=0$ ), which is filtered (to obtain angular spectrum of object wavefront at the hologram plane) and then propagated to the image plane using free space propagation function

The scattered wavefront's spatial frequency spectrum at the hologram plane is represented by

$$\hat{U}(f_x, f_y; z=0) = \int_{-\infty}^{\infty} \int_{-\infty}^{\infty} U(x, y, z=0) \exp[i2\pi(f_x x + f_y y)] dx dy \quad (4.5)$$

In the above equation  $\hat{U}(f_x, f_y; z=0)$  represents the FT of the complex amplitude distribution of the reference wavefront of the scattered reference wavefront at the hologram plane, with  $f_x$  and  $f_y$  representing the spatial frequencies in the x and y direction respectively. Fig 4.6 (b) shows the angular spectrum of the hologram in Fig 4.6 (a). This is a self-referencing off-axis hologram recorded with a Digital Holographic Microscopy employing a Fresnel biprism and a He-Ne laser. A random linearly polarized He-Ne ( $\lambda = 635\text{nm}$ , power  $< 2\text{mW}$ ) was used as a source. A CCD (Charged Couple Device) (Thorlabs, 8 bit,  $4.65\mu\text{m}$  pixel pitch) was used as a recording medium. Polystyrene microspheres of  $15\mu\text{m}$  diameter was used as an object (RI=1.58) which is immersed in microscope immersion oil (RI=1.518). The object is imaged using a MO (20x, NA 0.40).

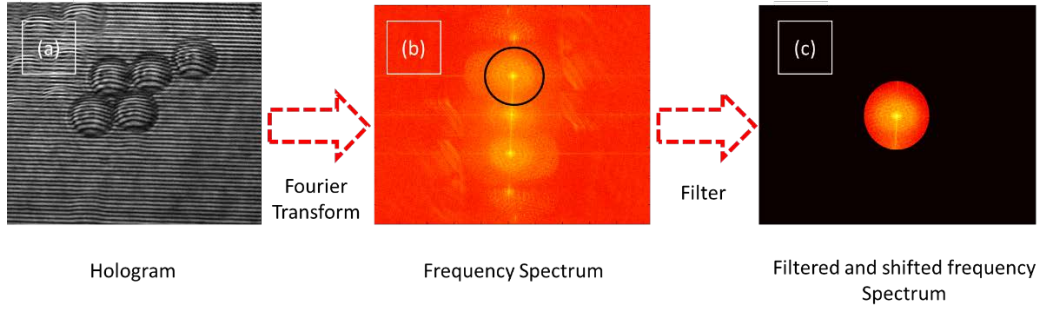


Fig 4. 6 (a) Hologram illuminated by the reference wavefront. (b) Power spectrum of the hologram obtained after Fourier transform, where three components (un-diffracted reference, real object and virtual object) can be seen. (c) Filtered spectrum, which contains only the spatial frequencies corresponding to object alone. This is then propagated to the image plane

To remove the unwanted terms (first and last terms from Eq. 4.3), which correspond to the un-diffracted reference wave and a distorted real object respectively, a circular band pass filter is applied to the resulting spectrum (Fig. 4.6 (b)). With the means of the filtering, spectral information corresponding to the object can be extracted and propagated. The complicated function is decomposed in a series of simple harmonic functions with the help of the Fourier transform (FT). Therefore, the inverse FT of the filtered spectrum of Eq. (4.5) provides the complex amplitude at  $(x,y,z=0)$  which contains only the object information (Fig. 4.6 (c)). This can be represented as [182,273].

$$\bar{U}(x, y, z = 0) = \int_{-\infty}^{\infty} \int_{-\infty}^{\infty} \text{filt}[\hat{U}(f_x, f_y; z = 0)] \exp[i2\pi(f_x x + f_y y)] df_x df_y \quad (4.6)$$

where  $\bar{U}(x, y, z = 0)$  is filtered (modified) complex amplitude distribution (containing only object information) and  $\text{filt}[\hat{U}(f_x, f_y; z = 0)]$ , is the filtered angular spectrum of  $U(x, y, z = 0)$ . If the complex amplitude at a plane parallel to the  $(x, y)$  plane but a distance  $z = d$  from the  $(x, y, z = 0)$  plane is known, then the angular spectrum at this plane can be written as [182]

$$\hat{U}(f_x, f_y; z = d) = \int_{-\infty}^{\infty} \int_{-\infty}^{\infty} U(x, y, z = d) \exp[-i2\pi(f_x x + f_y y)] dx dy \quad (4.7)$$

If one can determine the association between the angular spectrums at  $(x, y, z = 0)$  and  $(x, y, z = d)$ , then one can determine the influence of wave propagation on the angular spectrum. So the object complex amplitude distribution at  $(x, y, z = d)$  can be denoted in terms of its angular spectrum [182]

$$U_o(x, y, z = d) = \int_{-\infty}^{\infty} \int_{-\infty}^{\infty} \hat{U}(f_x, f_y; z = d) \exp[i2\pi(f_x x + f_y y)] df_x df_y \quad (4.8)$$

The solution of this wave field that satisfies the Helmholtz equation, can be written in terms of filtered spatial frequency distribution at the hologram plane as [273]

$$\hat{U}_o(f_x, f_y; z = d) = \text{filt}[\hat{U}(f_x, f_y; z = 0)] \exp\left[ik\sqrt{1 - \lambda^2 f_x^2 - \lambda^2 f_y^2} d\right] \quad (4.9)$$

The variation in the relative phases of the different constituents of the angular spectrum is nothing but the effect of propagation over a distance  $z=d$ . Between the two parallel planes (hologram and image), each plane wave components travels at a different angle, hence propagates to different distances, producing phase delays. In Eq. (4.9),  $\lambda$  is the vacuum wavelength of the light that illuminates the hologram. Inverse Fourier transform of Eq. (4.9) provides the complex amplitude at  $(x, y, z=d)$  as [273]

$$U_o(x, y, z = d) = \int_{-\infty}^{\infty} \int_{-\infty}^{\infty} \bar{U}(f_x, f_y; z = 0) \exp\left[ik\sqrt{1 - \lambda^2 f_x^2 - \lambda^2 f_y^2} d\right] \exp\left[i2\pi(f_x x + f_y y)\right] df_x df_y \quad (4.10)$$

The above relationship can be numerically implemented by Fourier transforming the wave field at the hologram plane, filtering it and multiplying it with the free space propagation function (first exponential function in the above equation) and then taking its inverse Fourier transform. Eq. (4.10) can then be written as [273]

$$U_o(x, y, z = d) = \mathfrak{F}^{-1}\left\{\mathfrak{F}\{U(x, y, z = 0)\} \exp\left[ik\sqrt{1 - \lambda^2 f_x^2 - \lambda^2 f_y^2} d\right]\right\} \quad (4.11)$$

The object's complex amplitude distribution at the image plane can be retrieved using the numerical reconstructions of holograms recorded with the DHM discussed in Eq. (4.11). If the hologram plane (digital array) is at the image plane of the magnifying lens, then  $d = 0$  and Eq. (4.11) reduces just to Fourier fringe analysis [256].

#### 4.4 Retrieval of intensity and phase of object wavefront

Complex amplitude at the image plane is numerically computed using Eq. (4.11). The most important parameter in quantitative phase imaging modality like DHM is the phase of the object wavefront. Eq. (4.11) can be used to retrieve the intensity and phase information of the object. The intensity of the wavefront is equal to the absolute square of the complex amplitude and can be represented as

$$I_o(x, y) = |U_o(x, y)|^2 \quad (4.12)$$

Phase of the object wavefront is calculated from the angle the complex amplitude makes with the real axis.

$$\phi_o(x, y) = \arctan \frac{\text{Im}[U_o(x, y)]}{\text{Re}[U_o(x, y)]} \quad (4.13)$$

For each object hologram, a background hologram usually known as reference hologram (Fig. 4.7 (b)), (the object is absent in the field of view and only the medium surrounding the object is present) and by keeping all the other parameters same, is also recorded. This hologram is also reconstructed using Eq. (4.11) and the phase is retrieved

$$\phi_B(x, y) = \arctan \frac{\text{Im}[U_B(x, y)]}{\text{Re}[U_B(x, y)]} \quad (4.14)$$

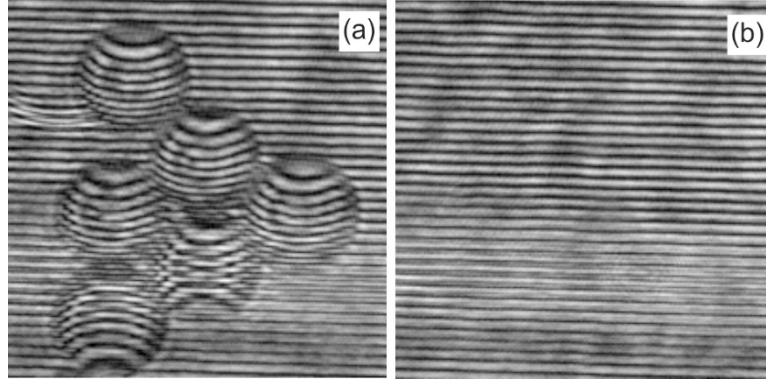


Fig 4.7 Object hologram of the 15μm diameter polystyrene sphere immersed in oil. (b) Background hologram (microscope immersion oil)

#### 4.5 Phase difference and object thickness

Phase difference (interference phase) is computed by deducting the background phase distribution from the object phase distribution [67]

$$\begin{aligned} \Delta\phi(x, y) &= \phi_o(x, y) - \phi_B(x, y) && \text{if } \phi_o > \phi_B \\ &= \phi_o(x, y) - \phi_B(x, y) + 2\pi && \text{if } \phi_B > \phi_o \end{aligned} \quad (4.15)$$

This phase subtraction nullifies the phase aberrations due to optical elements, as the parameters other than the object remained same between the exposures. This highlights only the phase distribution of the object alone, negating the phase present due to aberrations [63]. The phase difference acquired by the object beam that passes through the object is given by Eq. (4.15). This phase difference is proportional to both the refractive index (RI) difference between the sample and the surrounding medium (background) and the thickness of the object itself [63,78,80].

$$\Delta\phi(x, y) = \frac{2\pi}{\lambda}(n_o - n_B)L(x, y) \quad (4.16)$$

In Eq. (4.16), the constant average RI of the object and the background are  $n_o$  and  $n_B$  respectively and the spatially changing thickness of the object is represented by  $L$ . Eq. (4.16) can also be represented as

$$\Delta\phi(x, y) = \frac{2\pi}{\lambda}\Delta n L(x, y) \quad (4.17)$$

In Eq. (4.17),  $\Delta n$  is the RI difference between the object and the background. The spatially varying optical path length ( $OPL = \Delta n \times L$ ) distribution is either due to a spatial variation in RI or the or due to a spatially varying thickness. In the cells investigated, the spatial variation in

OPL is brought about by spatial variation in thickness rather than RI, which could be assumed to be a constant. If the RI values are known, then Eq. (4.16) can be used to construct the thickness distribution (3D image) of the object. Fig. 4.8 shows the 3D shape measurement of the 15 $\mu\text{m}$  diameter polystyrene microspheres using DHM. In the thickness reconstructions,  $n_o = 1.58$  and  $n_b = 1.518$  are used.

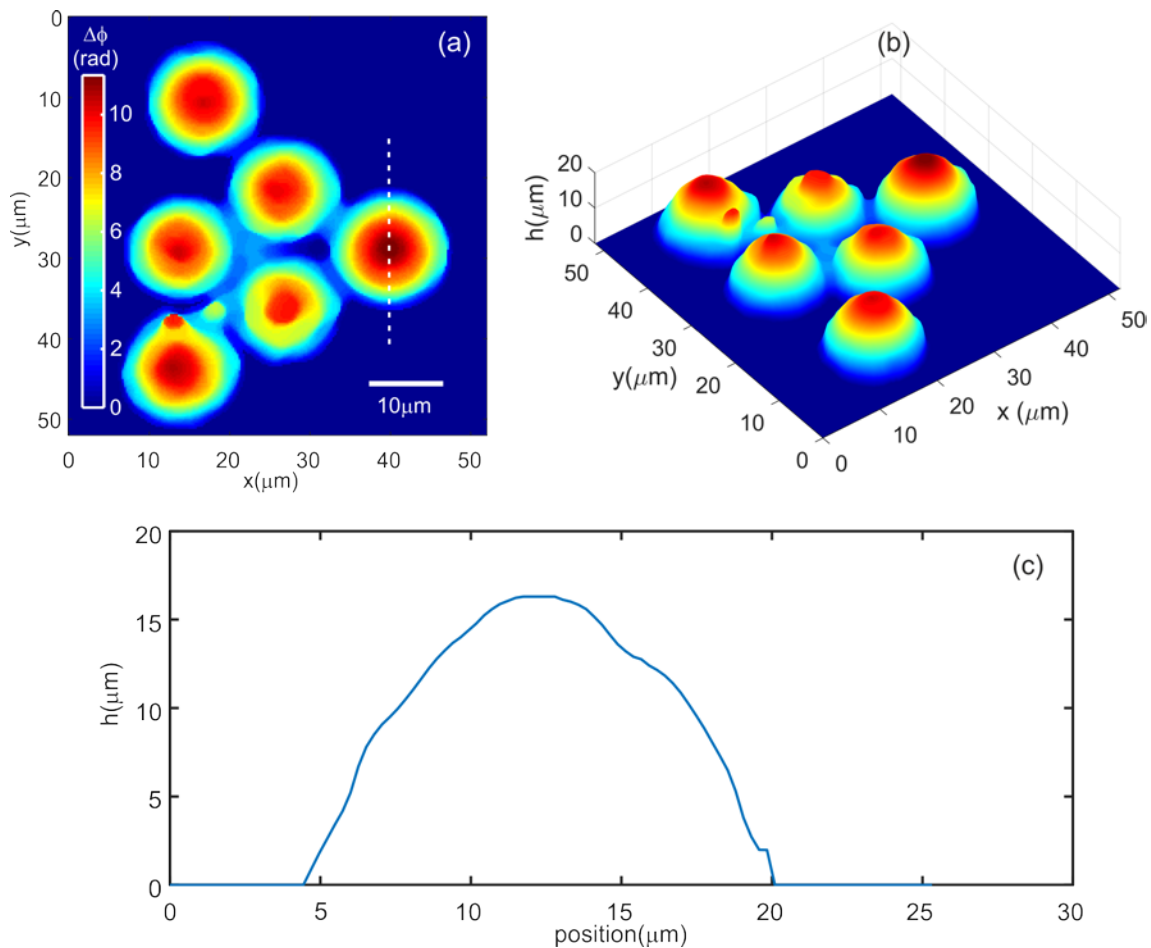


Fig 4.8 Quantitative phase reconstruction from digital holograms. (a) Continuous phase difference obtained in the case of 15 $\mu\text{m}$  diameter polystyrene microspheres. (b) Thickness distribution of the micro-sphere obtained by using the refractive index difference in Eq. (4.17). (c) Cross sectional thickness profile of the microsphere along the dashed line in Fig. 4.8a

Fig 4.8 summarizes the quantitative phase imaging by numerical reconstruction of digital holograms. Object and background holograms are reconstructed by the numerical implementation of Eq. (4.11). Eq. (4.13) and Eq. (4.14) are used to calculate the object and background phase respectively using their reconstructed complex amplitude distributions at the image plane. Then the phase difference is computed to annul the aberrations and to bring out the object phase distribution using Eq. (4.15). Continuous phase difference after phase unwrapping is shown in Fig. 4.8a. The obtained phase difference along with the RI values are

plugged into Eq. (4.17), to construct the object thickness profiles shown in Fig 4.8b and Fig 4.8c. It should also be noted that by changing the value of  $d$  in Eq. (4.11) information at different object planes can be obtained (even though path integrated), which might provide important object information, useful in its identification [78].

For the DHM techniques discussed in this thesis, Angular Spectrum Propagation integral given in Eq. 4.11, is used for the numerical reconstructions of holograms. The resulting phase images are used to compute the object thickness as well as its time evolution. Also, various static and dynamic parameters for the object under investigation are extracted from the reconstructed thickness profiles. In many cases, especially in the case of object identification and comparison, it is not necessary to have the RI values of the cell and the background medium. Optical path length profiles are sufficient to quantify, compare and identify object using DHM [53].